GM-CSF and IL-3 expression increases immune engraftment and tumor infiltration in a humanized patient-derived xenograft model of hepatocellular carcinoma

Kelley Weinfurtner[1], David Tischfield[2], George McClung[2], Jennifer Crainic[2], Jing Jiao[2], Wuyan Li[2], Erena Supan[2], David E. Kaplan[1,3], Terence P.F. Gade[2,3]

[1]Department of Gastroenterology and Hepatology, University of Pennsylvania
[2]Department of Radiology, University of Pennsylvania
[2]Department of Gastroenterology and Hepatology, University of Pennsylvania
[3]Corporal Michael J Cresenz VA Medical Center, Philadelphia, PA

Manuscript type: Research
Word count:

Conflicts of interest: The authors have declared that no conflict of interest exists.

Corresponding author: Terence P. F. Gade
Assistant Professor of Radiology and Cancer Biology
University of Pennsylvania Perelman School of Medicine
652 BRB II/III
421 Curie Blvd
Philadelphia, PA 19104-6160
Tel: 215-573-9756
Fax: 215-746-5511
Email: tgade@pennmedicine.upenn.edu

ABSTRACT

Introduction: Immunotherapy has shown promising results in hepatocellular carcinoma (HCC), but relevant model systems are greatly needed to inform treatment paradigms. Transplantation of immunodeficient mice with human hematopoietic cells allows for the development of humanized patient derived xenografts (HIS PDXs); however, these models have limited development of myeloid lineages. We aimed to determine the impact of human GM-CSF and IL-3 expression on tumor immune cell infiltration and tumor growth in a HIS PDX model of HCC.

Materials and Methods: HIS HCC PDXs were generated using NOG (NOD/Shi-*scid*/IL-2Rγ^{null}) and NOG-EXL (huGM-CSF/huIL-3 NOG) mice conditioned with 30mg/kg Busulfan and, 24 hours later, injected with 300,000 CD34+ cells isolated from human fetal livers. HCC tumor tissue from an established PDX line in Matrigel was then implanted subcutaneously (SQ). Immune engraftment was monitored by flow cytometry. Mice were sacrificed when tumors reached 2cm and tumor, blood, liver, and spleen were analyzed by flow cytometry.

Results: HIS NOG-EXL HCC mice demonstrated earlier and persistently increased huCD45+ peripheral blood immune cells compared to HIS NOG HCC mice with 12.1% vs 1.7% at tumor implantation ($p<0.0001$) and 82.1% vs 43.8% at steady state ($p<0.0001$). All major immune cell types were represented in both groups. There was no difference in tumor growth between HIS NOG HCC, HIS NOG-EXL HCC, and control NOG HCC tumors by latency (45.5, 50.5 days, and 48.4, respectively, $p=0.63$) or doubling time (8.6, 9.8, and 8.4 days, respectively, $p=0.63$). At necropsy, HIS NOG-EXL HCC mice had increased huCD45+ immune cells in tumor (57.6% vs 30.2% of live cells, $p=0.04$) compared to HIS NOG HCC mice with increased CD4+ regulatory T cells (14.6% vs 6.8% of T cells, $p=0.047$), CD4+ T cell PD-1 expression (84.7% vs 32.0% of CD4+ cells, $p<0.01$), and tumor-associated macrophages (1.2% vs 0.6% of CD45+ cells, $p<0.01$). Adult human bone marrow cells can be used as an alternative source of CD34+ cells and allow for partial HLA-matching to PDX tumor; however, an increased number of cells is required to maintain similar levels of engraftment.

Conclusions: HIS HCC PDX models demonstrate robust immune infiltration in the peripheral blood, spleen, liver, and HCC tumor. Expression of human GM-CSF and IL-3 lead to increased tumor infiltrating immune cells with a higher proportion of regulatory immune cells, suggesting NOG-EXL mice may be a more appropriate model for preclinical trials with immunotherapy.

INTRODUCTION

Hepatocellular carcinoma (HCC) is a leading cause of cancer-related mortality worldwide, as the majority of patients present with unresectable disease at diagnosis and a median survival of less than two years[1,2]. This dismal prognosis underscores the limited therapeutic options for this population. Recently, immunotherapy has emerged as a first line therapy for advanced HCC; however, regimens remain suboptimal due to low response rates and high rates of adverse effects.[3] Biomarkers of response to immunotherapy, such as PD-1/PD-L1 expression and tumor mutational burden, have been valuable in other malignancies, but have not proven predictive of response in HCC.[4] Early data suggests that immune cell phenotyping of HCC tumors may identify patients with greater likelihood of response to immunotherapy[5,6]; however, further understanding of the interaction of the immune microenvironment and immunotherapy outcomes is limited by the paucity of animal models that can recapitulate the heterogeneity of these factors present in human HCC.

Genetically engineered mouse (GEM) models can be highly useful to study the impact of a single or combined genetic alterations on tumor development and biology, but they lack the heterogeneity and complexity of genetic and epigenetic alterations present in human HCC.[7,8] Chemotaxic models allow for tumors to develop in a background of chronic liver disease as they do in patients, leading to greater genetic diversity and increased fidelity to the tumor microenvironment seen in patients, noting that tumorigenesis will be more variable and potentially time consuming. In both models, tumor formation occurs in immunocompetent mice, allowing for investigations into interactions between HCC tumors and the immune system with several important limitations. First, there can be major differences in the druggability of immunotherapy targets between human and murine homologs, and many of the FDA-approved immunotherapies do not bind the equivalent mouse targets.[9] Second, GEM tumors tend to be nonimmunogenic and often require additional strategies to mimic human immunosurveillance and immunotherapy responses.[10,11] Lastly, while the murine immune system has been used

frequently as a proxy for the human immune system, there are notable known and likely unknown differences in both innate and adaptive immunity.[12]

Patient-derived xenograft (PDX) models, in which human tumors are implanted into highly immunodeficient mice, have been shown to be representative of the heterogeneity of human tumors and patient response to therapy, making them important tools for preclinical therapeutic trials.[13,14] HCC PDXs have been described, but have largely been generated from patients with surgically cured, early-stage disease - likely to reflect less aggressive HCC variants that may never require systemic therapies such as immunotherapy. More recently, our lab and others have demonstrated the ability to generate HCC PDXs from biopsy samples, allowing for the development of PDX lines from patients with intermediate and advanced HCC – the patient population that will be considered for immunotherapy.[15.16] However, the lack of immune system in these models limit their utility in modeling interactions with the immune system and response to immunotherapies.

To overcome this limitation, immunodeficient mice can be xenotransplanted with human hematopoietic stem and progenitors cells to generate mice with humanized immune systems (HIS).[17-19] Engrafting human CD34+ cells into Nod-*scid* IL2Rγ^{null} (NSG) or NOD/Shi-*scid*/IL-2Rγ^{null} (NOG) immunodeficient mice results in HIS mice that produce all lineages of hematopoietic cells, including both innate and adaptive immune cells. While myeloid progenitor cells engraft well in the bone marrow, there are low rates of mature myeloid cells in the periphery of these mice, including cells important for HCC-immune interaction such as macrophages, neutrophils, and dendritic cells.[19-20] Further, the only published model of HCC in HIS mice demonstrated that the presence of HCC tumors leads to significant decrease in all human cells in the periphery.[21] The expression of various human cytokines has been shown to alter the proportion and functionality of different immune cell populations. Specifically, the expression of human granulocyte-macrophage colony-stimulating factor (GM-CSF) and interleukin-3 (IL-3) increases not only overall hematopoietic cell engraftment, but also leads to a

3-fold increase in myeloid cells in the periphery.[22-24] Interestingly, expression of these cytokines also leads to increased infiltration of regulatory T cells into all compartments, including tumor microenvironments.[22] We aimed to investigate what impact the expression of these cytokines has on HCC tumor growth and tumor immune infiltration in order to optimize HIS HCC PDX for the studies of the tumor immune microenvironment and response to immunotherapies.

RESULTS

NOG-EXL mice have increased peripheral immune engraftment, especially myeloid lineages

HIS NOG-EXL mice demonstrated earlier and persistently increased huCD45+ peripheral blood immune cells compared to HIS NOG HCC mice with 12.1% vs 1.7% of cells at 4 weeks post-implantation ($p<0.0001$) and 82.1% vs 43.8% of cells at steady state ($p<0.0001$, **Figure 1A**). All major immune cell types were represented in both groups, including B cells, T cells, NK cells, monocytes, dendritic cells, and neutrophils (**Figure 1B, Supp Figure 1A-F**). HIS NOG-EXL mice had a 2.0-fold increase in B cells, 2.7-fold increase in neutrophils, and 5.5-fold increase in monocytes in the peripheral blood compared to NOG mice at 9 weeks post-humanization, though no difference in total number of T cells, NK cells, or dendritic cells (**Figure 1C-H**). Human immune cells were also found in the liver (7.5% vs 3.2% of cells, $p=0.004$) and spleen (90.4% vs 73.2% of cells, $p=0.01$) of both HIS NOG and HIS NOG-EXL mice, respectively (**Figure 1I-J**) with increased total number of all major immune cells except similar number of dendritic cells in HIS NOG-EXL mice compared to HIS NOG mice (**Supp Figure 1G-R)**. As seen in the peripheral blood, HIS NOG-EXL mice also had a proportional increase in monocytes (3.8% vs 0.7% of huCD45+ cells, $p<0.01$) and neutrophils (3.3% vs 1.5% of huCD45+ cells, $p<0.01$) in the liver compared to HIS NOG mice (**Figure 1K-P**). Notably, there was no difference in T cell subtypes (CD4+, CD8+, Th1, Th17, Treg, naïve, effector) or PD-1 expression between the two cohorts in liver, spleen, or peripheral blood (**Supp Figure 2**).

Humanized immune system does not impact subcutaneous PDX engraftment or tumor growth rates

All HCC tumor implanted subcutaneously (SQ) engrafted regardless of mouse background (8/8 for HIS NOG, 5/5 for HIS NOG-EXL, **Figure 2A**). There was no difference in tumor growth by latency (48.4, 45.5, and 50.5 days, p=0.63) or doubling time (8.4, 8.6, and 9.8 days, respectively, p=0.63) in control NOG, HIS NOG, and HIS NOG-EXL, respectively (**Figure 2B-D**). Orthotopic tumors only engrafted in only 3/8 (37.5%) of HIS NOG mice and 0/4 (0%) HIS NOG-EXL mice compared to 2/3 (66.7%) in NOG control (**Supp Figure 3a)**. For the tumors that did grow, there was no difference in latency or standardized growth rates (data not shown). Implanting PDX tumors orthotopically at 2 weeks rather than 4 weeks post-humanization improved engraftment significantly (4/5, 80.0% vs 0/5, 0% in HIS NOG-EXL, p<0.01, **Supp Figure 3b**), suggesting an immune cell-mediated suppression of tumor growth not seen in the subcutaneous compartment.

HIS NOG-EXL mice have increased tumor immune infiltration with a higher proportion of regulatory immune cells

At necropsy, HIS NOG-EXL mice had increased huCD45+ immune cell infiltration into SQ HCC tumors compared to HIS NOG mice as measured by flow cytometry (57.6% vs 30.2% of live cells, p=0.04) and immunohistochemistry (117.3 vs 36.4 cells/HPF, p=0.02, **Figure 2E-K**). This included increased overall T cell infiltration (flow cytometry: 9.8% vs 23.1% of live cells, p=0.04, and IHC: 14.8 vs 3.3 cells/HPF, p=0.02) with proportionally increased CD4+ cells (70.8% vs 51.3% of T cells, p=0.03), CD4+ regulatory T cells (14.6% vs 6.8% of T cells, p=0.047), and CD4+ T cell PD-1 expression (84.7% vs 32.0% of CD4+ cells, p<0.01). HIS NOG-EXL mice also have a proportional increase in tumor-associated macrophages (TAMs, flow cytometry: 1.2% vs 0.6% of CD45+ cells, p<0.01, IHC: 32.8 vs 3.4 cells/HPF, p=0.02, **Figure 2L-M**).

Presence of HCC tumor influences systemic cytokine and immune cell populations

The presence of HCC tumor did not impact overall peripheral blood chimerism in humanized mice (42.8% vs 40.5% in HIS NOG HCC vs sham mice, p=0.80; 68.4% vs 67.1% in HIS NOG-EXL HCC vs sham mice, p=0.71; **Figure 3A**); however, it did increase the proportion of circulating monocytes (2.0% vs 1.1% in HIS NOG mice, p=0.047; 3.8% vs 3.2% in HIS NOG-EXL mice, p=0.19; **Figure 3B-C**), neutrophils (0.7% vs 0.3% in HIS NOG mice, p<0.01; 1.1% vs 0.8% in HIS NOG-EXL mice, p=0.16; **Figure 3D-E**), and NK cells (1.7% vs 0.7% in HIS NOG mice, p=0.20; 0.9% vs 0.3% in HIS NOG-EXL mice, p=0.02; **Figure 3F-G**).

Adult bone marrow CD34+ cells allow for partial HLA-matching but require more cells to maintain circulating immune cells

Adult bone marrow (BM) CD34+ cells were obtained from Ossium Health and partially match by human leukocyte antigen (HLA)-typing to PDX tumor with priority given to matching at least one allele of *HLA-A*, HLA-B* and HLA-DRB1**. When compared to using 300,000 fetal liver (FL)-derived CD34+, at least 500,000 adult BM-derived CD34+ cells were required to reach similar number of human immune cells in peripheral blood by week 9 post-humanization (42.0%, 49.1%, 59.4% vs 67.7% huCD45+ cells for 100,000, 200,000, 500,000 BM CD34+ cells vs 300,000 FL CD34+ cells, respectively, p<0.0001, **Figure 4A-D**). Even more notable, there was a significant decrease in circulating human immune cells after week 10 when using BM C34+ cells (28.2%, 25.8%, 41.8% vs 72.3% huCD45+ cells at week 12 for 100,000, 200,000, 500,000 BM CD34+ cells vs 300,000 FL CD34+ cells, respectively, p<0.0001). At least 500,000 BM CD34+ were needed to consistently maintain chimerism past 14 weeks. Notably, the mice with decreasing chimerism in the peripheral blood had a significantly higher proportion of monocytes than FL CD34+ control (17.7% vs 5.0% at week 9, p<0.0001).

DISCUSSION

Here we demonstrate a novel HIS HCC PDX model using NOG-EXL mice that express human GM-CSF and IL-3. These mice demonstrate robust immune infiltration with increased number of circulating human immune cells in the peripheral blood, as well as increased human immune

cell infiltration into spleen, liver, and HCC tumor. Notably, this included a high proportion of regulatory immune cells in the HCC tumor microenvironment, including increased Tregs, CD4+PD1+ T cells, and TAMs. We also demonstrated that the presence of an HCC tumor changes the concentrations of circulating human chemokines in the peripheral blood and peripheral blood cell populations that were not specific to mouse background but did lead to significantly higher circulating monocytes and neutrophils in EXL mice than humanized mice not expressing human GM-CSF and IL-3.

The only other published humanized HCC PDX model demonstrated that humanization of NSG mice increases growth rates and size of HCC tumors. In our cohorts, the presence of HIS did not impact SQ HCC tumor growth as determined by engraftment, latency, or doubling time, but, notably, decreased orthotopic engraftment significantly in both NOG and NOG-EXL mice. Differences due to mouse background are unlikely as NOG mice are functionally equivalent to NSG mice. The improvement in orthotopic engraftment with earlier implantation and trend to increase immune infiltration in orthotopic tumors compare to SQ tumors support the hypothesis that impaired engraftment is at least in part due to the presence of the immune system. One potential consideration is the degree of alloimmune response given in our experiment CD34+ cells derived from FL were not HLA-matched, while Zhao et al partially matched CD34+ cells to PDX tumors.

In addition, our cohorts had consistent number of circulating immune cells once plateau was reached; however, Zhao et al report a peak of huCD45+ cells in peripheral blood at 2 weeks post-HCC implantation and a 5-fold decrease by 8 weeks post-implantation. Again, a major difference between studies was partial-HLA matching; however, our cohorts using partially-matched adult BM CD34+ cells had peak of huCD45+ cells in peripheral blood at 7 weeks post-implantation in both HCC and sham controls, suggesting it was related to the CD34+ site and not presence of tumor.

There are important limitations of this model, noting that all mice eventually die of anemia and macrophage activation syndrome (MAS). While published data suggests these mice begin to die at 15 weeks post-humanization, in our hands, mice consistently survive past 20 weeks. Degree of anemia is correlated with amount of chimerism, so optimizing models to increase tissue immune infiltration with similar BM engraftment will help solve this problem. Newer immunodeficient mice that have knocked in human cytokines to mouse cytokine loci, including M-CSF, GM-CSF, IL-3, TPO, IL-6, SIRPa (ie MISTRG and MISTRG-6 mice), have demonstrated acceptable tissue immune infiltration with chimerism less than 30%. These models also allow autologous mobilized peripheral blood to be utilized with multilineage hematopoiesis without graft versus host disease. Unfortunately, these models are not commercially available at this time.

CONCLUSIONS

HIS HCC PDX models demonstrate robust immune infiltration in the peripheral blood, spleen, liver, and HCC tumor. Expression of human GM-CSF and IL-3 lead to increased tumor infiltrating immune cells with a higher proportion of regulatory immune cells, suggesting NOG-EXL mice may be a more appropriate model for preclinical trials with immunotherapy.

MATERIALS AND METHODS

Humanized mice

NOG (NOD.Cg-*Prkdc*^{scid} *Il2rg*^{tm1Sug}) or NOG-EXL [NOD.Cg-*Prkdc*^{scid} *Il2rg*^{tm1Sug} Tg(SV40/HTLV-IL3,CSF2)] mice were obtained from Taconic and human fetal liver-derived CD34+ hematopoietic stem/progenitor cells were obtained from the University of Pennsylvania's Stem Cell Xenograft Core. The mice were conditioned with intravenous (i.v.) injection of 35 mg/kg busulfan and then injected with 300,000 human CD34+ cells by tail vein 24 hours later.

Humanized HCC PDX generation

HCC PDX was generated from percutaneous biopsy of a patient's HCC tumor implanted into NSG mice and serially passaged as previously described.[16] Immune engraftment was confirmed by the presence of human CD45+ cells in the peripheral blood at 4 weeks post-CD34+ cell transplant. HCC PDX tissue was then implanted with Matrigel subcutaneously (SQ) into the flank or orthotopically into the liver of the humanized mice and growth monitored with calipers or ultrasound, respectively. Sham implantations with Matrigel only were also implanted SQ or orthotopically. Mice were sacrificed once the tumor reached 20 mm in any direction or at end of experiment if no tumor growth.

Immune cell analysis by flow cytometry

Immune engraftment was monitored by flow cytometry on peripheral blood samples obtained from retro-orbital collection every 2 weeks. At necropsy, peripheral blood, tumor, liver, and spleen were harvested. Tissue was mechanically dissociated through 70 micron filter and all samples underwent lysis of red blood cells with ACK lysis buffer prior to antibody staining using the antibodies listed in supplemental table 1. Flow cytometry panels were analyzed using the gating strategies shown in supplemental figure 1.

Immunohistochemistry analysis

At necropsy, portions of tumor, liver, and spleen were fixed in formalin for subsequent paraffin embedding. Tissue was stained using antibodies for total human cells (huCD45***), T cells (huCD3+), cytotoxic T cells (huCD8+), B cells (huCD19+), natural killer cells (huCD56+), and macrophages (huCD68+), as listed in supplemental table 2. Cell per high power field (HPF) were averaged from ***.

Cytokine/chemokine analysis

Plasma was obtained from biweekly peripheral blood samples collected as previously discussed. Cytokine and chemokine concentrations were determined using a custom Luminex assay from Bio-Techne that included beads for CCL2, CCL4, CCL5, CCL20, CXCL1, CXCL5, CXCL10, CXCL13, granzyme A, GM-CSF, IL-2, IL-3, IL-4, IL-5, IL-6, IL-10, IL-12, IL-17/IL-17A, interferon-gamma, and TNF-alpha, as well as the following angiokines – angiopoietin-1, angiopoietin-2, Tie-2, and VEGF.

Statistics

Study approval

All manipulations with mice were approved by Institutional Animal Care and Use Committee at our institution. All animal experimental procedures were conducted in accordance with the approved protocols and Guide for the Care and Use of Laboratory Animals.

Data availability

Individual FCS files for flow analysis and other primary data can be accessed from corresponding author on request.

AUTHOR CONTRIBUTIONS

KW: designed research studies, conducted experiments, analyzed data, wrote the manuscript

DT: carried out experiments, analyzed data, revised manuscript

JC: carried out experiments, revised manuscript

WL: carried out experiments, revised manuscript

DK: designed research studies, revised manuscript

TG: designed research studies, analyzed data, revised manuscript

ACKNOWLEDGEMENTS

Research reported in this publication was supported by Penn Center for Precision Medicine Accelerator Grant and VA CSR&D I01 CX-001933. KW is supported by CTSA KL2 Mentored Career Development Award. The authors would also like to acknowledge the Stem Cell Xenograft Core (RRID: SCR_010035), the Center for Molecular Studies in Digestive and Liver Diseases (P30DK050306), and the Molecular Pathology and Imaging Core (RRID: SCR_022420).

REFERENCES

1. Bray, F. *et al.* Global cancer statistics 2018: GLOBOCAN estimates of incidence and mortality worldwide for 36 cancers in 185 countries. *CA. Cancer J. Clin* 2018; 68: 394–424.
2. Park, J. W. *et al.* Global patterns of hepatocellular carcinoma management from diagnosis to death: The BRIDGE Study. *Liver Int.* 2015;35:2155–2166.
3. Finn, R. S. *et al.* Atezolizumab plus Bevacizumab in Unresectable Hepatocellular Carcinoma. *N. Engl. J. Med.* 2020;382:1894–1905.
4. Pinter, M., Jain, R. K. & Duda, D. G. The Current Landscape of Immune Checkpoint Blockade in Hepatocellular Carcinoma: A Review. *JAMA Oncol.* 2021;7(1):113-123.
5. Sia, D. *et al.* Identification of an Immune-specific Class of Hepatocellular Carcinoma Based on Molecular Features. *Gastro*. 2017;153:812-826.
6. Llovet, J. M., Montal, R., Sia, D. & Finn, R. S. Molecular therapies and precision medicine for hepatocellular carcinoma. *Nat Rev Clin Oncol*. 2018;15:599–616.
7. Brown, Z. J., Heinrich, B., & Greten, T. F. Mouse models of hepatocellular carcinoma: an overview and highlights for immunotherapy research. *Nat Rev Gastro Hep.* 2018;15:536-554.
8. Olson, B., Li, Y., Lin, Y., Liu, E. T., & Patnaik, A. Mouse models for cancer immunotherapy research. *Cancer Discov.* 2018; 1358-1365.
9. Magiera-Mularz, K. et al. Human and mouse PD-L1: similar molecular structure, but different druggability profiles. *iScience*. 2020;24(1):101960.
10. Ruiz de Galarreta, M. et al. B-catenin activation promotes immune escape and resistance to anti-PD-1 in hepatocellular carcinoma. *Cancer Discov.* 2019;9(8):1125-1141.
11. Wang, J. et al. UV-induced somatic mutations elicit a functional T cell response in the YUMMER1.7 mouse melanoma model. *Pigment Cell Melanoma Res*. 2017;30(4):428-435.
12. Mestas, J. and Hughes, C. C. W. Of mice and not men: differences between mouse and human immunology. *J. Immun*ol. 2004;172:2731-2738.

13. Gao H. et al. High-throughput screening using patient-derived tumor xenografts to predict clinical trial drug response. *Nat Med.* 2015;21:1318–25.

14. Byrne, A. T. et al. Interrogating open issues in cancer precision medicine with patient-derived xenografts. *Nat. Rev. Cancer.* 2017;17(4):254-268.

15. Blumer, T. et al. Hepatocellular Carcinoma Xenografts Established From Needle Biopsies Preserve the Characteristics of the Originating Tumors. *Hepatol. Commun.* 2019;3:971–986.

16. Tischfield, D. et al. Establishment of Hepatocellular Carcinoma Patient-Derived Xenografts from Image-Guided Percutaneous Biopsies. *Sci Rep*. 2019;9:10546.

17. Yahata, T. et al. Functional human T lymphocyte development from cord blood CD34+ cells in nonobese diabetic/Shi-scid, IL-2 receptor null mice. *J. Immunol*. 2002;169:204–209.

18. Shultz L. D. et al. Human lymphoid and myeloid cell development in NOD/LtSz-scid IL2R gamma null mice engrafted with mobilized human hemopoietic stem cells. *J Immunol*. 2005;174:6477–89.

19. Shultz L. D. et al. Humanized mice for immune system investigation: progress, promise and challenges. *Nat Rev Immunol.* 2012;12:786–98.

20. Tanaka, S. et al. Development of mature and functional human myeloid subsets in hematopoietic stem cell-engrafted NOD/SCID/IL2ryKO mice. *J Immunol.* 2012;188(12):6145-6155.

21. Zhao, Y. et al. Development of a new patient-derived xenograft humanised mouse model to study human-specific tumour microenvironment and immunotherapy. *Gut.* 2018;67:1845–1854.

22. Bilerbeck, E. et al. Development of human CD4+FoxP3+ regulatory T cells in human stem cell factor-, granulocyte-macrophage colony-stimulating factor-, and interleukin-3-expressing NOD-SCID IL2R-gamma(null) humanized mice. *Blood*. 2011;117(11):3076-3086.

23. Maser, I. P. et al. The tumor milieu promotes functional human tumor-resident plasmacytoid dendritic cells in humanized mouse models. *Front Immunol.* 2020:11;2082.

24.

15. Zhao, Y. et al. Analysis and Validation of Human Targets and Treatments Using a Hepatocellular Carcinoma Immune Humanized Mouse Model. *Hepatol.* 2021;74:1395-1410.

16. Maser, I. et al. The Tumor Milieu Promotes Functional Human Tumor-Resident Plasmacytoid and Dendritic Cells in Humanized Mouse Models. *Front Immuno.* 2020;11:2082.

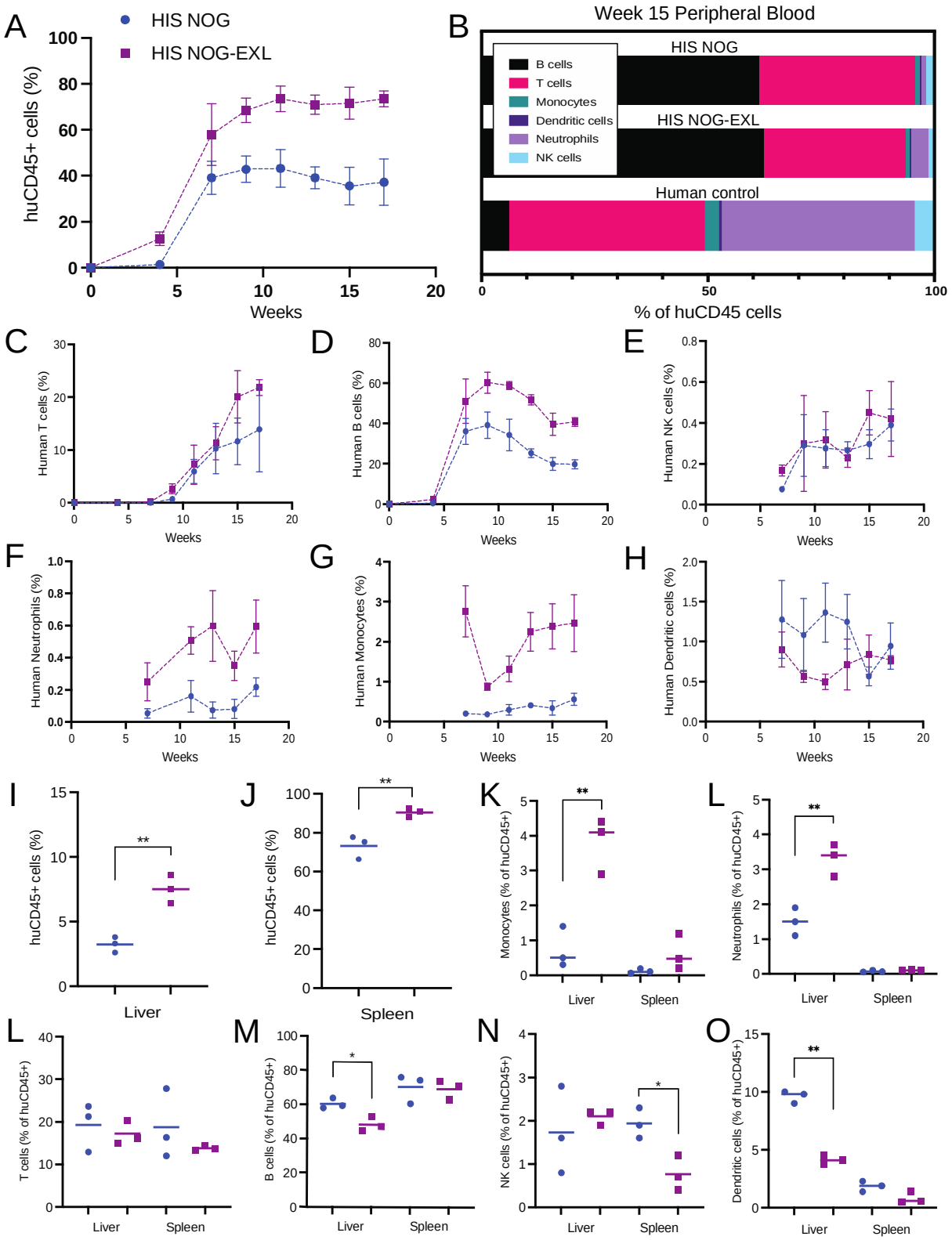
A
HIS NOG
HIS NOG-EXL
huCD45+ cells (%)
Weeks
B
Week 15 Peripheral Blood
HIS NOG
HIS NOG-EXL
Human control
B cells
T cells
Monocytes
Dendritic cells
Neutrophils
NK cells
% of huCD45 cells
C
Human T cells (%)
D
Human B cells (%)
E
Human NK cells (%)
F
Human Neutrophils (%)
G
Human Monocytes (%)
H
Human Dendritic cells (%)
I
huCD45+ cells (%)
J
huCD45+ cells (%)
K
Monocytes (% of huCD45+)
L
Neutrophils (% of huCD45+)
L
T cells (% of huCD45+)
M
B cells (% of huCD45+)
N
NK cells (% of huCD45+)
O
Dendritic cells (% of huCD45+)
Liver
Spleen

Figure 1: s

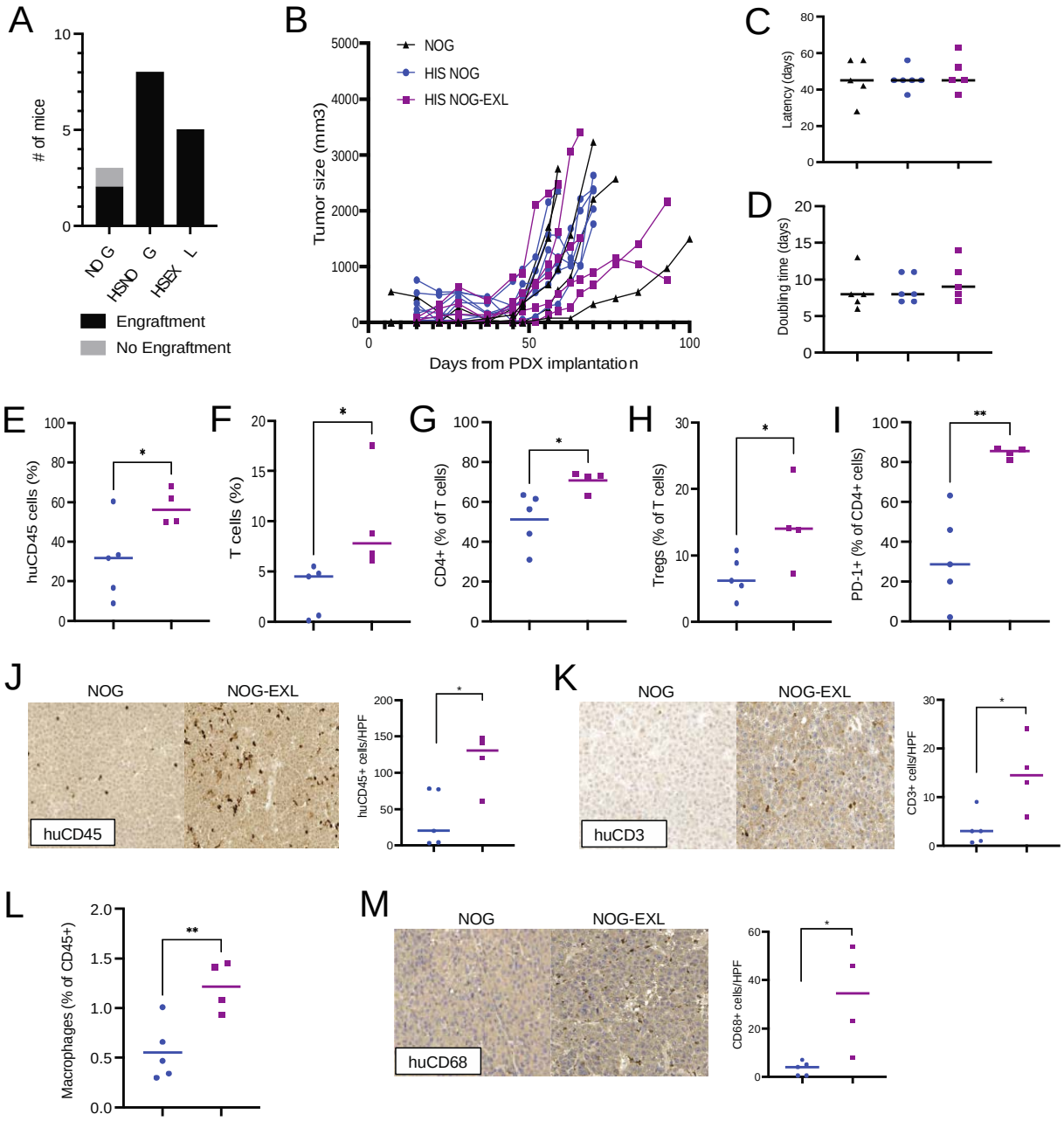
A
# of mice
NOG
HSNOG
HSEXL
Engraftment
No Engraftment
B
Tumor size (mm3)
NOG
HIS NOG
HIS NOG-EXL
Days from PDX implantation
C
Latency (days)
D
Doubling time (days)
E
huCD45 cells (%)
F
T cells (%)
G
CD4+ (% of T cells)
H
Tregs (% of T cells)
I
PD-1+ (% of CD4+ cells)
J
NOG
NOG-EXL
huCD45
huCD45+ cells/HPF
K
NOG
NOG-EXL
huCD3
CD3+ cells/HPF
L
Macrophages (% of CD45+)
M
NOG
NOG-EXL
huCD68
CD68+ cells/HPF

Figure 2: s

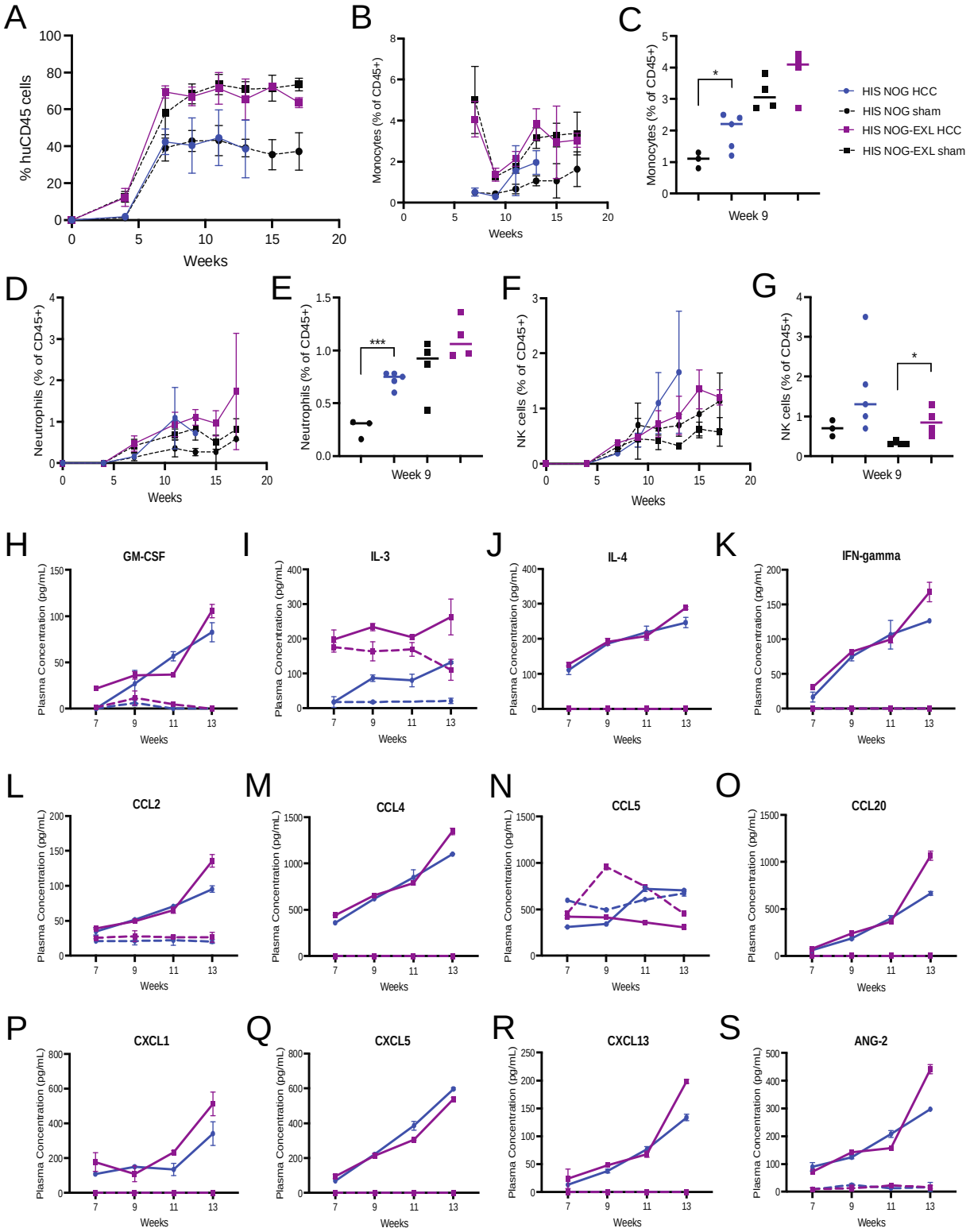
A
% huCD45 cells
Weeks
B
Monocytes (% of CD45+)
Weeks
C
Monocytes (% of CD45+)
Week 9
HIS NOG HCC
HIS NOG sham
HIS NOG-EXL HCC
HIS NOG-EXL sham
D
Neutrophils (% of CD45+)
Weeks
E
Neutrophils (% of CD45+)
Week 9
F
NK cells (% of CD45+)
Weeks
G
NK cells (% of CD45+)
Week 9
H
GM-CSF
I
IL-3
J
IL-4
K
IFN-gamma
L
CCL2
M
CCL4
N
CCL5
O
CCL20
P
CXCL1
Q
CXCL5
R
CXCL13
S
ANG-2
Plasma Concentration (pg/mL)
Weeks

Figure 3: s

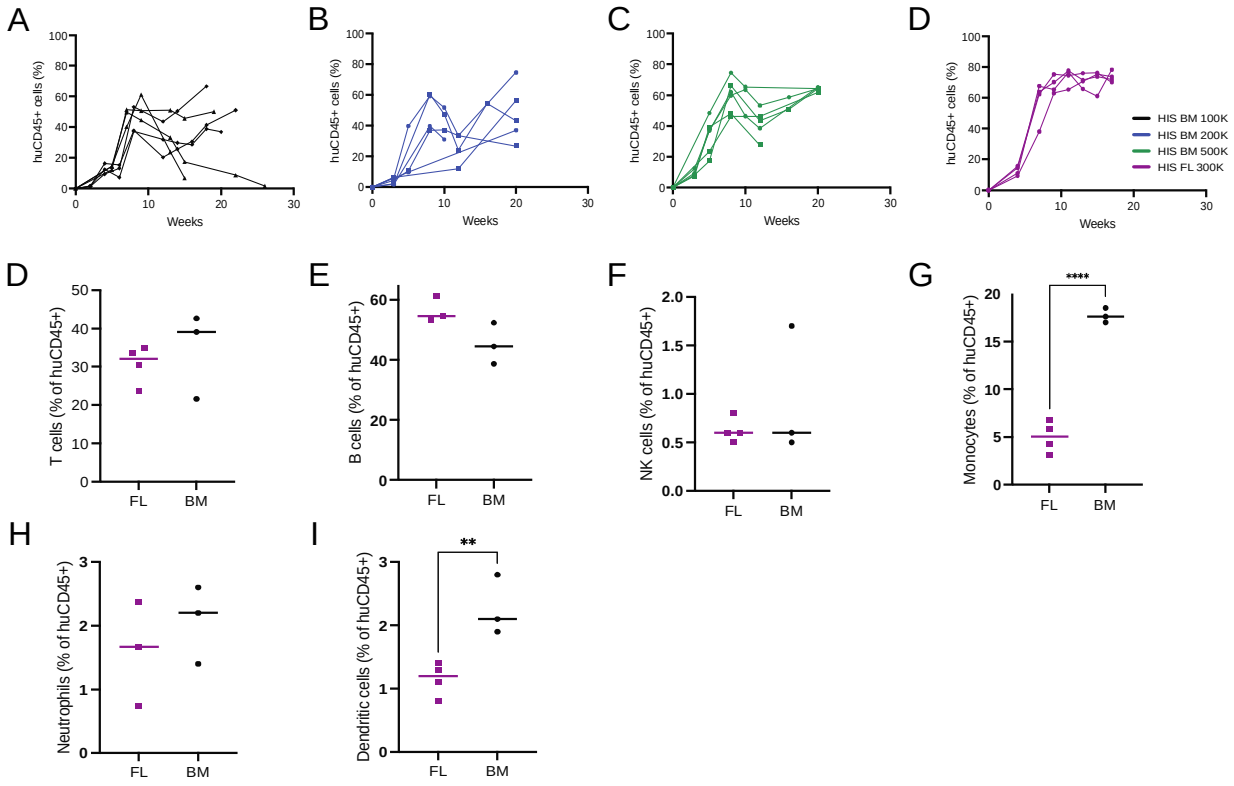
A
B
C
D
huCD45+ cells (%)
Weeks
HIS BM 100K
HIS BM 200K
HIS BM 500K
HIS FL 300K
D
E
F
G
H
I
T cells (% of huCD45+)
B cells (% of huCD45+)
NK cells (% of huCD45+)
Monocytes (% of huCD45+)
Neutrophils (% of huCD45+)
Dendritic cells (% of huCD45+)
FL
BM
****
**

Figure 4:

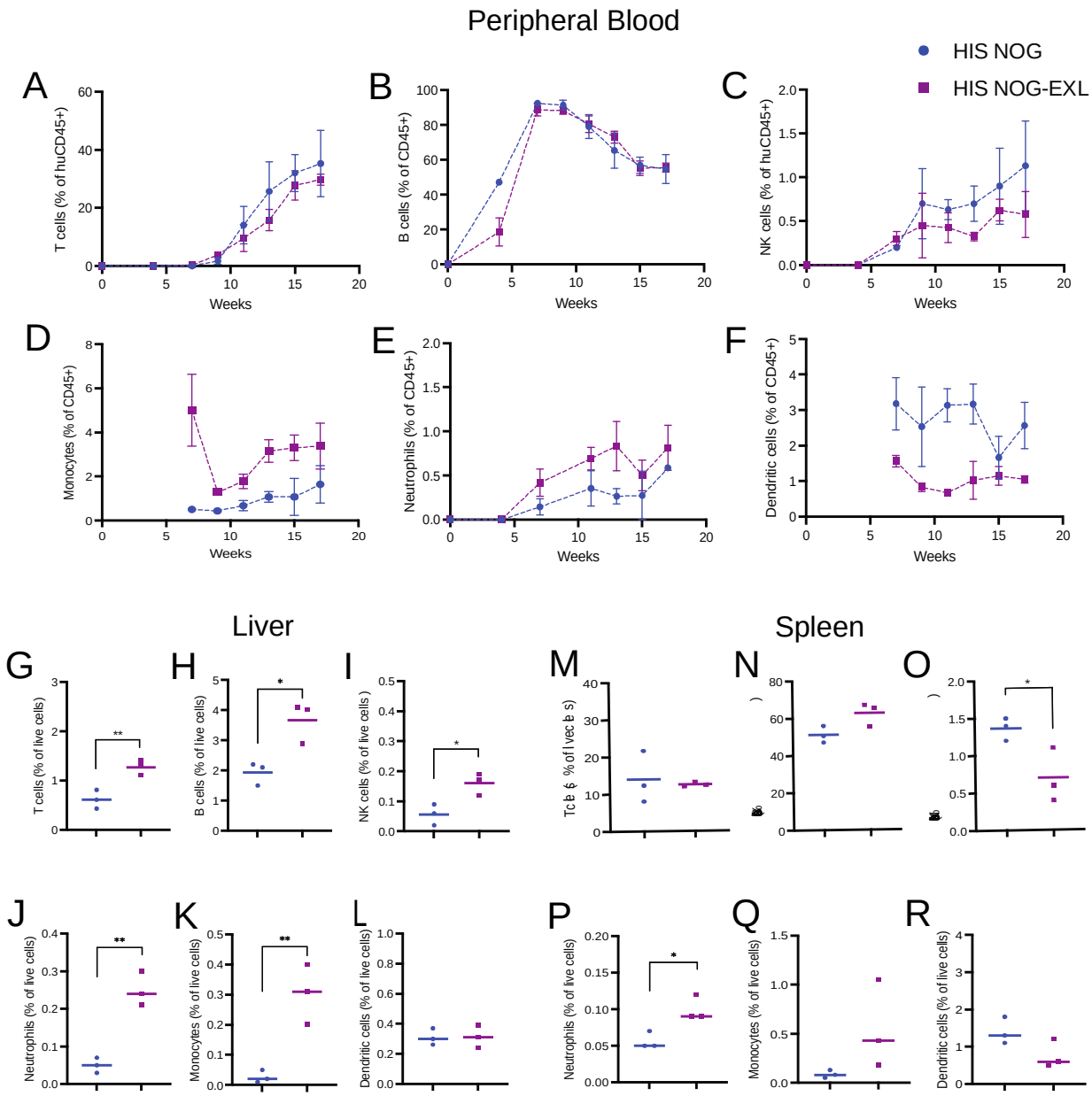

Supplementary Figure 1:

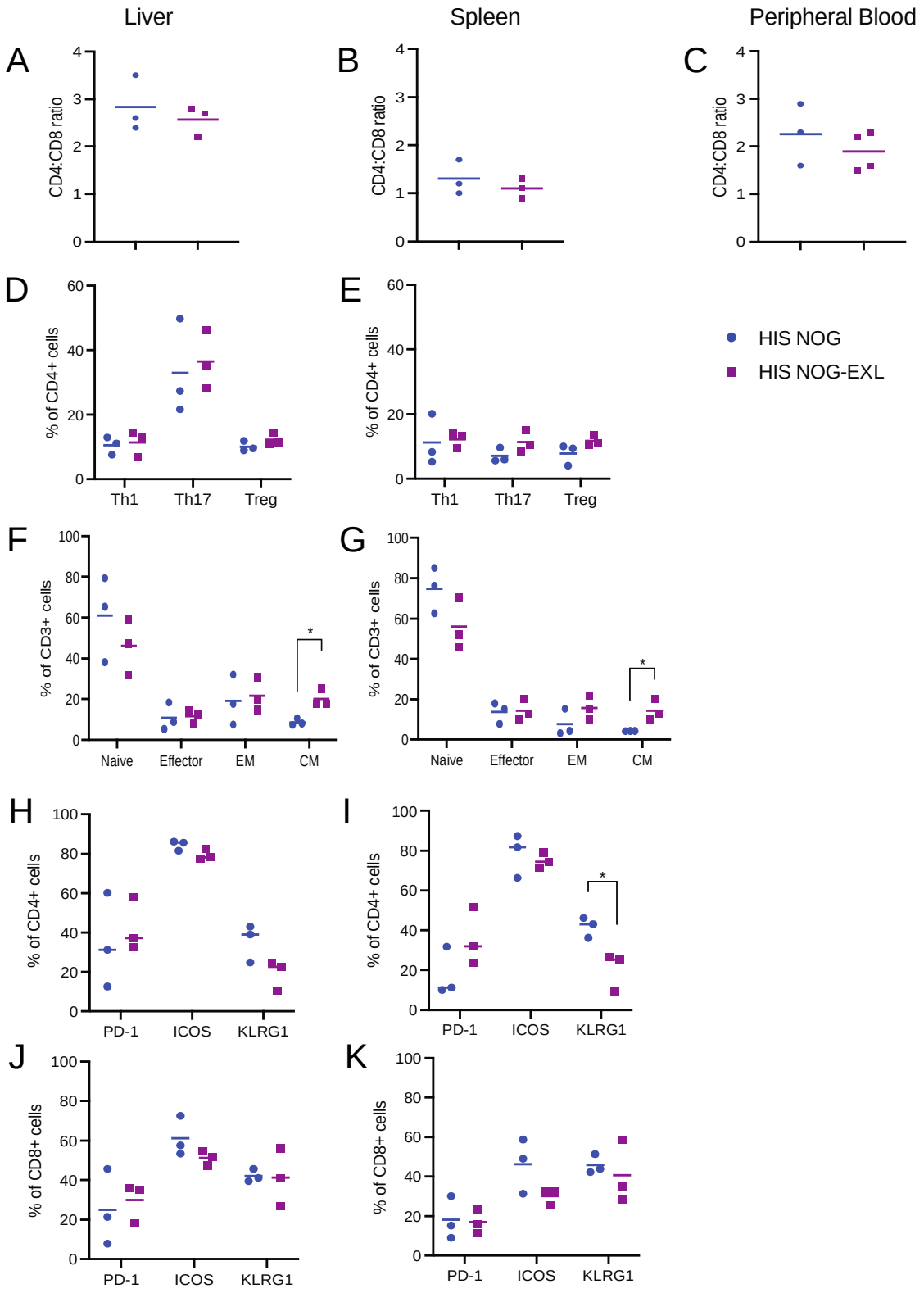

Supplementary Figure 2: